Short Papers

Adaptive Fuzzy Hysteresis Internal Model Tracking Control of Piezoelectric Actuators With Nanoscale Application

Pengzhi Li, Peiyue Li, and Yongxin Sui

***Abstract*—In this paper, a novel Takagi–Sugeno (T–S) fuzzy-system-based model is proposed for hysteresis in piezoelectric actuators. The antecedent and consequent structures of the developed fuzzy hysteresis model (FHM) can be identified online through uniform partition approach and recursive least squares (RLS) algorithm, respectively. With respect to the controller design, the inverse of FHM is used to develop a fuzzy internal model (FIM) controller. Decreasing the hysteresis effect, the FIM controller has a good performance of high-speed trajectory tracking. To achieve nanometer-scale tracking precision, the novel fuzzy adaptive internal model (FAIM) controller is uniquely developed. Based on real-time input and output data to update FHM, the FAIM controller is capable of compensating for the hysteresis effect of the piezoelectric actuator in real time. Finally, the experimental results for two cases are shown: the first is with 50 Hz and the other with multiple-frequency (50 + 25 Hz) sinusoidal trajectories tracking that demonstrate the efficiency of the proposed controllers. Especially, being 0.32% of the maximum desired displacement, the maximum error of 50-Hz sinusoidal tracking is greatly reduced to 6 nm. This result clearly indicates the nanometer-scale tracking performance of the novel FAIM controller.**

***Index Terms*—Fuzzy adaptive internal model (FAIM), hysteresis, piezoelectric actuator, Takagi–Sugeno (T–S), trajectory tracking.**

I. Introduction

The lead-zirconate-titanate piezoelectric ceramics (PZT) in use today are mainly $PbTiO_3$–$PbZrO_3$ compounds. The piezoelectric actuator (also referred as PZT) is mainly composed of piezoelectric ceramics. Because of its high bandwidth, nanometer displacement resolution, and zero mechanical friction, the piezoelectric actuator is widely used in micro/nanomanipulation [1], micro/nanopositioning [2]–[4], and optics [5], [6]. However, the intrinsic nonlinear and multivalued hysteresis in the piezoelectric actuator has the potential to cause inaccuracy or even instability of its applied system. The maximum error resulting from the hysteresis can be as much as 10–15% of the path covered [7].

The hysteresis is often characterized by nonlinearity and rate dependence. Nonlinearity means that the same input voltage results in different output displacements during the course of voltage increase and decrease. There is no one-to-one relationship between voltage and displacement. Besides, rate dependence indicates that the frequency of input voltage has influence on the shape and orientation of hysteresis curve.

Over the past decade, many models such as Preisach model [8], [9], Prandtl–Ishlinskii (PI) model [10], Maxwell slip model [11], Duhem model [12], [13], and Jiles–Atherton model [14] have been presented mainly for rate-independent hysteresis. For rate-dependent hysteresis, the authors of [15]–[17] proposed several modified PI models combining neural network or a density function of time rate of input. Recently, autoregressive-moving-average-based [18] model and automatic real-time vision-based [19] method were developed for hysteresis in piezoelectric actuators. Feedforward controller, feedback controller, and complex controller with both feedforward and feedback schemes have also been developed for hysteresis compensation in the piezoelectric actuator. Tien *et al.* [20] showed that iterative inversion-based feedforward control could be used to compensate for the dynamics-coupling error in piezoscanners during high-speed positioning. Sliding-mode control strategies [21]–[23] were adopted for trajectory tracking of the piezoelectric actuator. Nguyen and Choi[24] proposed a closed-loop rate-independent hysteresis compensator for a stacked PZT actuator from a congruency-based hysteresis model. Support vector machine model-based complex controller [25] was designed to suppress the rate-dependent hysteresis.

Among many control schemes, internal model control has displayed a conspicuous popularity in process control industry due to its good robustness against disturbances and model mismatch [26], [27]. The basic structure of an internal model control scheme is usually composed of the internal model controller, the plant, the plant model, and the feedback filter. In fact, the determination of the plant model plays an important role in the development of internal model control. The internal model controller can be directly obtained via the inversion of the plant model. The feedback filter is generally designed to alleviate sensitivity problems. If the plant model matches the plant exactly, a perfect disturbance rejection and trajectory tracking will be achieved. Thus, the major task of an internal model control scheme is to find a precise plant model.

Recently, a fuzzy system has been broadly utilized in nonlinear modeling [28]–[31] and automatic control [32]–[35]. This paper proposes a simple Takagi–Sugeno (T–S) [36], [37] fuzzy-system-based model for both rate-independent and rate-dependent hysteresis. The fuzzy hysteresis model (FHM) uses uniform partition approach and recursive least squares (RLS) algorithm for identification and optimization. The inverse of FHM is used to design a fuzzy internal model (FIM) controller to decrease the hysteresis effect. To achieve nanometer-scale tracking precision, the novel fuzzy adaptive internal model (FAIM) controller is uniquely developed. For two cases of periodic trajectories tracking, experimental results demonstrate the efficiency of the proposed controllers.

Manuscript received April 7, 2015; revised June 6, 2015 and August 10, 2015; accepted November 3, 2015. Date of publication November 20, 2015; date of current version October 4, 2016. This work was supported by the National Key Scientific and Technological Special Project of China under Grant 2009ZX02205.

Pengzhi Li is with Changchun Institute of Optics, Fine Mechanics and Physics, Chinese Academy of Sciences, Changchun 130033, China, and also with the University of Chinese Academy of Sciences, Beijing 100049, China (e-mail: kindrobot@163.com).

Peiyue Li and Y. Sui are with the Changchun Institute of Optics, Fine Mechanics and Physics, Chinese Academy of Sciences, Changchun 130033, China.

Color versions of one or more of the figures in this paper are available online at http://ieeexplore.ieee.org.

Digital Object Identifier 10.1109/TFUZZ.2015.2502282

The organization of this paper is as follows. Section I gives a brief introduction. In Section II, the structure, identification, and inverse of FHM is proposed. Section III presents the developed controllers. Section IV includes the experimental setup and results. In Section V, a summary of the paper is given.

II. Fuzzy Hysteresis Model

Generally, a fuzzy system is composed of a fuzzifier, fuzzy rule base, fuzzy inference engine, and defuzzifier. The fuzzifier transforms real-valued input variables to fuzzy sets. The fuzzy rule base can be viewed as sets of many fuzzy IF–THEN rules. The fuzzy inference engine adopts individual rule or composition-based inference method to map fuzzy sets in the input universe of discourse $U \subset R^n$ to ones in the output universe of discourse $Y \subset R$ based on some fuzzy logic. The defuzzifier transforms fuzzy sets in $Y \subset R$ to real-valued output. Especially, without the fuzzifier and defuzzifier, the T–S fuzzy system has real-valued input and output variables. Appropriate for modeling nonlinear systems, it is chosen to model hysteresis in the piezoelectric actuator.

A. Fuzzy Hysteresis Model Structure

A discrete-time PZT system with hysteresis is considered. The T–S FHM has the following fuzzy rules:

$$\begin{aligned} &R^l: \text{ IF } y(k-1) \text{ is } A^l, \\ &\text{THEN } y(k) = q_{l1}y(k-1) + q_{l2}u(k) + q_{l3} \end{aligned} \tag{1}$$

where $y(k) = y(kT_\mathrm{s}) = y_k$ and $u(k) = u(kT_\mathrm{s}) = u_k$ are the output and input of PZT system at the time instant kT_s, respectively; T_s is the sampling period; $q_{l1}, q_{l2},$ and q_{l3} are real-valued parameters of the consequent part (i.e., THEN part of the fuzzy rule); $l = 1, \ldots, L$, L is the number of fuzzy rules.

A^l is a fuzzy set with triangular membership function $\mu_{A^l}(y_{k-1})$ defined as

$$\mu_{A^l}(y_{k-1}) = \begin{cases} 1 - |y_{k-1} - c_l|/a_l & y_{k-1} \in [c_l - a_l, c_l + a_l] \\ 0, & \text{otherwise} \end{cases} \tag{2}$$

where c_l and a_l are the parameters of the membership function in the premise part (i.e., IF part of the fuzzy rule). Compared with the Gaussian exponential membership function, the advantage of the triangular membership function lies in little computational burden without the loss of modeling accuracy.

The fuzzy basis function, which can also be referred as weighted firing strength, is given by

$$p^l(y_{k-1}) = \frac{\mu_{A^l}(y_{k-1})}{\sum_{l=1}^{L}\left(\mu_{A^l}(y_{k-1})\right)}. \tag{3}$$

Finally, the weighted average output $\hat{y}_k$ of FHM is

$$\hat{y}_k = \sum_{l=1}^{L}\left(p^l(y_{k-1})\left(q_{l1}y(k-1) + q_{l2}u(k) + q_{l3}\right)\right). \tag{4}$$

It should be noted that fuzzy rule of (1) is actually equivalent to the following one:

R^l: IF $y(k-1)$ is A^l and $u(k)$ is I^l, THEN $y(k) = q_{l1}y(k-1) + q_{l2}u(k) + q_{l3}, l = 1, \ldots, L$, where I^l is a fuzzy set with the membership function $\mu_{I^l}(u_k) = 1$. The advantages are as follows.

1) FHM identification of premise parameters is simplified without considering u_k.
2) The analytic inverse of FHM is easily obtained without u_k in the premise part of fuzzy rule.

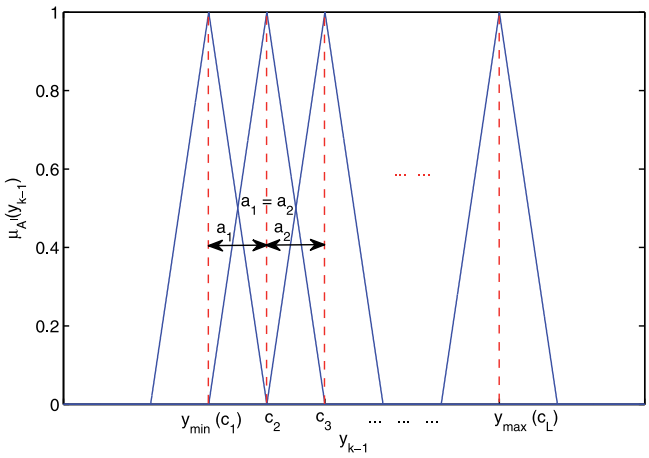

Fig. 1. Uniform partition of y_{k-1} in the premise part of FHM.

B. Fuzzy Hysteresis Model Identification

In order to solve the hysteresis problem of multivalued mapping, herein extended input variable is used. Suppose N pairs of experimental data $(y_k, u_k) = (y(k), u(k)), k = 1, \ldots, N$, have been sampled. The premise parameters c_l, a_l and consequent parameters $q_{l1}, q_{l2}, q_{l3}, l = 1, \ldots, L$, need to be identified for FHM.

For premise parameters $c_l, a_l, l = 1, \ldots, L$, due to the especially designed "partial" fuzzy rule, the input variable y_{k-1} is partitioned uniformly. Suppose numerical range of $y_{k-1}, k = 1, \ldots, N$, is $[y_{\min}, y_{\max}]$; then,

$$c_l = y_{\min} + (y_{\max} - y_{\min})(l-1)/(L-1) \tag{5}$$

$$a_1 = a_2 = \cdots = a_L = (y_{\max} - y_{\min})/(L-1). \tag{6}$$

Herein, the premise part of FHM has been obtained; that is to say, fuzzy sets $A^l, l = 1, \ldots, L$, have been known, illustrated as Fig. 1. The fuzzy sets are normal, complete, and consistent. This uniform partition method is computationally easier than both subtractive clustering and fuzzy C-means clustering algorithms. Besides, it can be applied online.

Next, the consequent parameters $q_{l1}, q_{l2}, q_{l3}, l = 1, \ldots, L$ are optimized by using RLS algorithm. The performance criterion is chosen as

$$J = \frac{1}{2}\sum_{k=1}^{N}\left(e_\mathrm{m}(k)\right)^2 = \frac{1}{2}\sum_{k=1}^{N}\left(y(k) - \hat{y}_k\right)^2. \tag{7}$$

The vectors for the consequent parameters and extended input can be defined as

$$\begin{aligned} \boldsymbol{q}_l &= [q_{l1}, q_{l2}, q_{l3}]^T, \boldsymbol{q}_l \in R^{3\times 1} \\ \tilde{\boldsymbol{u}}_k &= [y_{k-1}, u_k, 1]^T, \tilde{\boldsymbol{u}}_k \in R^{3\times 1} \\ \boldsymbol{q} &= \left[\boldsymbol{q}_1^T, \boldsymbol{q}_2^T, \cdots, \boldsymbol{q}_L^T,\right]^T, \boldsymbol{q} \in R^{(3L)\times 1} \\ \bar{\boldsymbol{u}}_k &= \left[p^1(y_{k-1})\tilde{\boldsymbol{u}}_k^T, p^2(y_{k-1})\tilde{\boldsymbol{u}}_k^T, \ldots, p^L(y_{k-1})\tilde{\boldsymbol{u}}_k^T\right]^T \\ \bar{\boldsymbol{u}}_k &\in R^{(3L)\times 1}. \end{aligned} \tag{8}$$

Then, $\hat{y}_k$ of (4) can be rewritten as

$$\begin{aligned}\hat{y}_k &= \sum_{l=1}^{L}\left(p^l(y_{k-1})\left(\boldsymbol{q}_l^T\cdot\tilde{\boldsymbol{u}}_k\right)\right)\\ &= p^1(y_{k-1})\tilde{\boldsymbol{u}}_k^T\cdot\boldsymbol{q}_1+p^2(y_{k-1})\tilde{\boldsymbol{u}}_k^T\cdot\boldsymbol{q}_2+\cdots\\ &\quad +p^L(y_{k-1})\tilde{\boldsymbol{u}}_k^T\cdot\boldsymbol{q}_L\\ &= \bar{\boldsymbol{u}}_k^T\cdot\boldsymbol{q}. \end{aligned}\tag{9}$$

Then, the RLS algorithm at each time instant $k=1,2,\ldots,N$ can be written as

$$\begin{aligned}\boldsymbol{q}(k) &= \boldsymbol{q}(k-1)+\mathbf{P}(k-1)\bar{\boldsymbol{u}}_k\frac{y(k)-\bar{\boldsymbol{u}}_k^T\cdot\boldsymbol{q}(k-1)}{\lambda+\bar{\boldsymbol{u}}_k^T\mathbf{P}(k-1)\bar{\boldsymbol{u}}_k}\\ \mathbf{P}(k) &= \left(\mathbf{I}-\frac{\mathbf{P}(k-1)\bar{\boldsymbol{u}}_k\bar{\boldsymbol{u}}_k^T}{\lambda+\bar{\boldsymbol{u}}_k^T\mathbf{P}(k-1)\bar{\boldsymbol{u}}_k}\right)\frac{\mathbf{P}(k-1)}{\lambda}\end{aligned}\tag{10}$$

where $\mathbf{P}\in R^{(3L)\times(3L)}$ and $\mathbf{I}\in R^{(3L)\times(3L)}$ is an identity matrix and $\lambda\in(0,1]$ is the forgetting factor. The initial parameters can be chosen as $\mathbf{P}(0)=\alpha\mathbf{I}$ and $\boldsymbol{q}(0)=\varepsilon[1,1,\ldots]^T$, respectively. α is a big positive constant value, and ε is a small positive constant or zero value. The RLS algorithm can be easily applied online. In the following paragraph, parameters are selected as $\lambda=1,\alpha=1\times10^6$ and $\varepsilon=0$.

C. Fuzzy Hysteresis Model Inverse

After the premise parameters c_l,a_l and consequent parameters $q_{l1},q_{l2},q_{l3},l=1,\ldots,L$, have been identified, from (4), the inverse u_{inv} of FHM can be analytically obtained.

Rewrite (4) as

$$\begin{aligned}&\hat{y}_k\left(\sum_{l=1}^{L}\left(\mu_{A^l}\left(y_{k-1}\right)\right)\right)\\ &=\sum_{l=1}^{L}\left(\mu_{A^l}(y_{k-1})\left(q_{l1}y(k-1)+q_{l2}u(k)+q_{l3}\right)\right)\\ &=u(k)\sum_{l=1}^{L}\left(\mu_{A^l}(y_{k-1})q_{l2}\right)\\ &+\sum_{l=1}^{L}\left(\mu_{A^l}(y_{k-1})\left(q_{l1}y(k-1)+q_{l3}\right)\right).\end{aligned}$$

Then, transpose it as

$$\begin{aligned}&u(k)\sum_{l=1}^{L}\left(\mu_{A^l}(y_{k-1})q_{l2}\right)\\ &=\hat{y}_k\left(\sum_{l=1}^{L}\left(\mu_{A^l}\left(y_{k-1}\right)\right)\right)\\ &-\sum_{l=1}^{L}\left(\mu_{A^l}(y_{k-1})\left(q_{l1}y(k-1)+q_{l3}\right)\right)\end{aligned}$$

finally, by substituting $u_{\mathrm{inv}}(k)$ for $u(k)$ and $y(k)$ for $\hat{y}_k$, the inverse of FHM can be attained as in (11), shown at the bottom of the page.

It implies that an inverse-model-based internal model controller can be designed to compensate for the nonlinear hysteresis effect of PZT system.

D. Fuzzy Hysteresis Model Computational Time Complexity

With regard to the modern digital signal processor (DSP), the computational time complexity [38] in this paper is approximately defined as how many multiplication and division operations performed during each sampling period by FHM. Denote $T(i)$ as the computational time complexity of the ith equation; then,

$$\begin{aligned}T(2) &= 1\\ T(4) &= 6L+1=O(L)\\ T(10) &= (3L)^3+4(3L)^2+5(3L)+2\\ &= 27L^3+36L^2+15L+2=O(L^3)\\ T(11) &= 7L+2=O(L).\end{aligned}\tag{12}$$

More details of the computational time complexity about the proposed controllers and its applications in the practical controller implementation will be given in Sections III and IV.

III. Tracking Controller Design

Fig. 2 shows the block diagram of the controller implementation. The module Z^{-1} represents one sampling period delay. The module *Fuzzy Internal Hysteresis Model* serves as the function of plant model, working according to (4). The module *Inverse Fuzzy Internal Model Controller* serves as the function of internal model controller, running according to (11). The module *Feedback Filter* is actually a low-pass filter and very important to the robustness of the overall controller. The module *Fuzzy Adaptive Hysteresis Model* uses real-time input and output of PZT stage to make FHM adapted to on-site hysteresis characteristics according to (5), (6), and (10).

In practical applications, FHM is never perfect, resulting in a nonnull error of model mismatch. The error may deteriorate performance or even cause instability of the overall controller. Hence, a filter is often added for robustness. With unit gain, the module *Feedback Filter* has the following discrete-time transfer function:

$$\frac{1-\beta}{1-\beta z^{-1}}=\frac{(1-\beta)z}{z-\beta}.\tag{13}$$

Generally, for closed-loop stability of the overall controller, the parameter β of the filter is chosen as $\beta\in(0,1)$.

For comparison, the conventional PID controller is also employed. It is widely used in industrial processes due to its simplicity, applicability, and ease of use [39]. Here, the discrete-time

$$u_{\mathrm{inv}}(k)=\frac{y(k)\left(\sum_{l=1}^{L}\left(\mu_{A^l}\left(y_{k-1}\right)\right)\right)-\sum_{l=1}^{L}\left(\mu_{A^l}(y_{k-1})\left(q_{l1}y(k-1)+q_{l3}\right)\right)}{\sum_{l=1}^{L}\left(\mu_{A^l}(y_{k-1})q_{l2}\right)}.\tag{11}$$

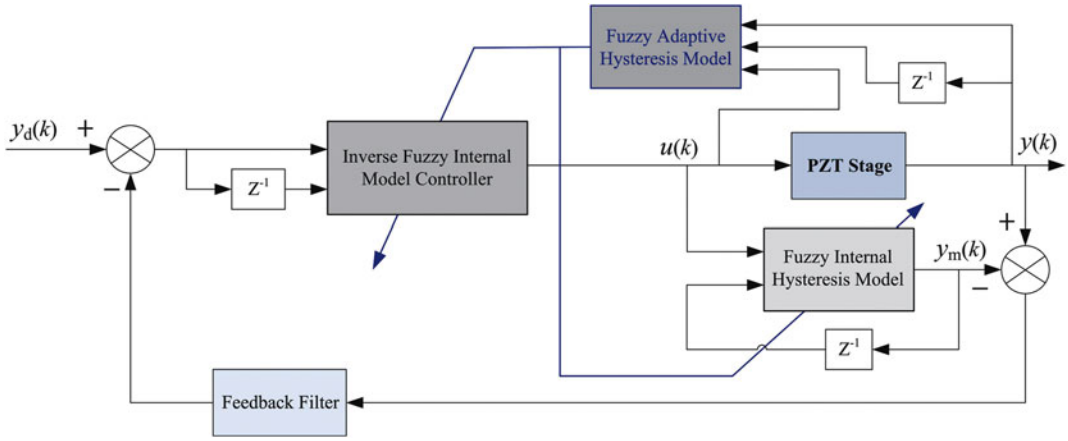

Fig. 2. Block diagram of the overall controller.

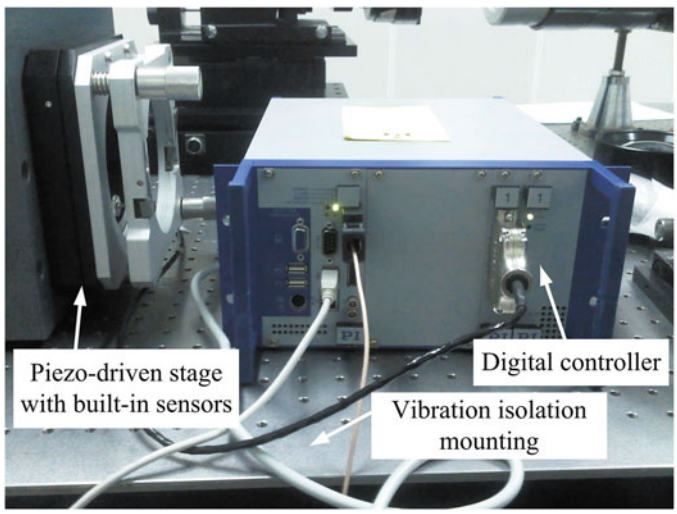

Fig. 3. Experimental platform driven by the piezoelectric actuator: the capacitive sensors are built in the piezo-driven stage; the floating-point DSP, voltage amplifier, signal conditioner, and A/D and D/A converters are all located in the digital controller.

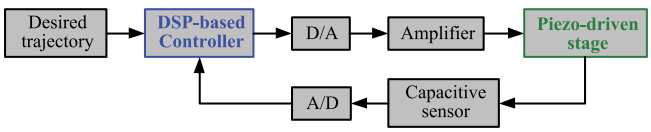

Fig. 4. Diagram of the experimental layout: the real-time displacement of the piezo-driven stage is measured by the capacitive sensor; with the input of the displacement and desired trajectory, the DSP-based controller implements the proposed FIM and FAIM control strategy; the output of the controller is amplified by the amplifier and then excites the piezo-driven stage.

incremental PID algorithm is adopted as follows:

$$\begin{aligned} u(k) &= u(k-1) + \Delta u(k) \\ \Delta u(k) &= k_{\mathrm{p}}\left(e(k) - e(k-1)\right) + k_{\mathrm{i}} e(k) \\ &\quad + k_{\mathrm{d}}\left(e(k) - 2e(k-1) + e(k-2)\right) \end{aligned} \tag{14}$$

where k_p, k_i, and k_d are the proportional gain, integral gain, and derivative gain, respectively. It is often a process of trial and error to find suitable or even optimum PID parameters.

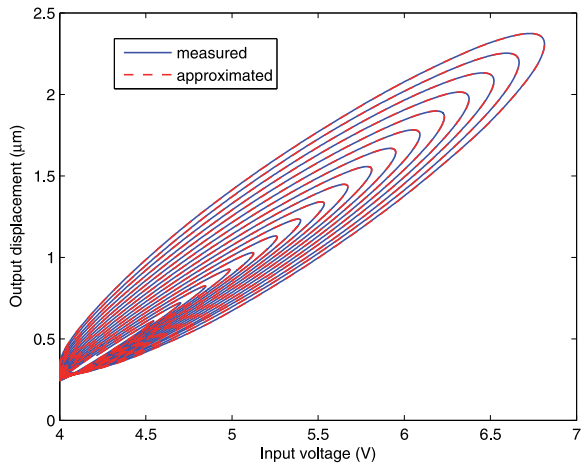

Fig. 5. Measured and approximated hysteresis curve on different input frequencies.

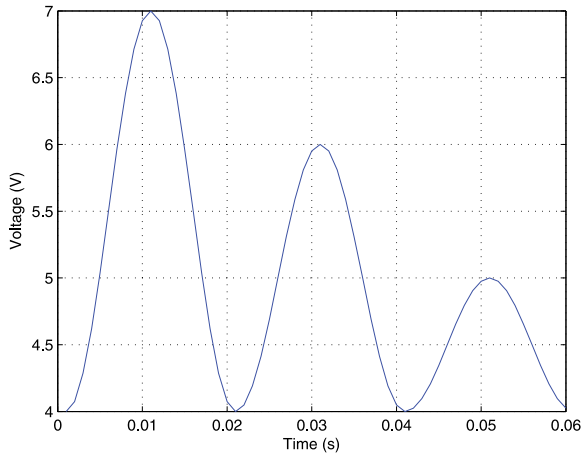

Fig. 6. Input voltage for FHM identification.

A. *Fuzzy Internal Model Controller*

Without the module *Fuzzy Adaptive Hysteresis Model* working, the overall controller is equivalent to an FIM controller. First, based on collected input and output data of PZT system, a suitable FHM is obtained offline in advance. Then, using the obtained FHM and its inverse, the modules *Fuzzy Internal Hysteresis Model* and *Inverse Fuzzy Internal Model*

Controller work, and the FIM controller tracks the desired trajectory y_d. Its tracking performance is mainly concerned with the generality and match precision of the obtained FHM. The computational time complexity of the FIM controller is $T_{\mathrm{FIM}} = T(4) + T(11) = 13L + 3 = O(L)$.

B. Fuzzy Adaptive Internal Model Controller

With the module *Fuzzy Adaptive Hysteresis Model* working, the overall controller acts as an FAIM controller. It can achieve better tracking performance than FIM controller due to the real-time updating of FHM. The working procedure of FAIM controller is as follows.

1) Use initial FHM identified offline to run the FIM controller for i periods of y_d.
2) Treat y_d as the input variable and then uniformly partition y_d according to (5) and (6) to obtain the premise parameters of future adaptive FHM.
3) During ith period, according to (10), use real-time input and output data of PZT system to update the consequent parameters at each time instant. After the ith period ends, notated as FHM_i, the adaptive FHM of ith period is obtained.
4) During the next period, i.e., $(i+1)$th period, use FHM_i to run the FAIM controller. Meanwhile, increase i by 1, execute 3) in parallel.
5) Return to 4) for the next period.

The following are some remarks about the design of FAIM controller.

1) The premise parameters of adaptive FHM are updated according to y_d, not real-time output y of PZT system. First, y_d are known in advance; therefore, this process needs to be updated just once. It can greatly reduce the real-time computational burden. Second, the control objective is to make y track y_d; therefore, it is reasonable to replace y with y_d.
2) As y_d are commonly periodic, the updating process, i.e., working of the module *Fuzzy Adaptive Hysteresis Model*, is executed every period of y_d. The data of only one period are used to update the FHM. That is to say, during $(i+1)$th period, the working modules *Fuzzy Internal Hysteresis Model* and *Inverse Fuzzy Internal Model Controller* are based on the updated FHM_i, and the updating FHM_{i+1} of current period is intended to change the FAIM controller of next period. First, for more general implementation, initial FHM and FIM controllers are not always optimum. Second, the updating of current FHM works in parallel with current FAIM controller and only affects it during next period. It can avert unnecessary oscillations and moreover reduce the real-time computational burden.
3) The computational time complexity of the FAIM controller is $T_{\mathrm{FAIM}} = T_{\mathrm{FIM}} + T(10) = 27L^3 + 36L^2 + 28L + 5 = O(L^3)$, which is considerably demanding. Its application in the practical implementation of FAIM controller will be discussed in Section IV.

C. Stability of the Controller

According to (4), the output $y(k)$ of PZT stage in Fig. 2 can be represented as

$$y(k) = \frac{\sum_{l=1}^{L}\left(\mu_{A^l}(y_{k-1})\left(q_{l1}y(k-1)+q_{l3}\right)\right)}{\sum_{l=1}^{L}\left(\mu_{A^l}(y_{k-1})\right)} + \frac{\sum_{l=1}^{L}\left(\mu_{A^l}(y_{k-1})q_{l2}\right)}{\sum_{l=1}^{L}\left(\mu_{A^l}(y_{k-1})\right)}u(k) + \xi(k) + d(k)$$
$$= f(y(k-1)) + g(y(k-1))u(k) + \xi(k) + d(k)$$
$$= f(k-1) + g(k-1)u(k) + \xi(k) + d(k) \tag{15}$$

where $\xi(k)$ is the modeling error of FHM, $d(k)$ is the noise and disturbance, and $f(\cdot)$ and $g(\cdot)$ are nonlinear functions of $y(k-1)$, respectively.

Assumption 1. The PZT stage is stable in the open loop, the stable inverse of FHM exists and $g \neq 0$.

Assumption 2. $|\xi(k)| \leq \xi_0$, $|d(k)| \leq d_0$, ξ_0 and d_0 are positive values, and $\bar{\xi} = \xi_0 + d_0$.

Based on Assumption 1, the control law $u(k)$ in Fig. 2 can be expressed as

$$u(k) = g^{-1}(k-1)\left(y_d(k) - f(k-1) - F(z)(\xi(k) + d(k))\right) \tag{16}$$

where $F(z)$ is the representation of the module *Feedback Filter*.

Define $e(k) = y_d(k) - y(k)$; then

$$e(k+1) = y_d(k+1) - y(k+1)$$
$$= y_d(k+1) - (f(k) + \xi(k+1) + d(k+1) + g(k)u(k+1)). \tag{17}$$

According to (16), (17) can be rewritten as

$$e(k+1) = y_d(k+1) - (f(k) + \xi(k+1) + d(k+1) + g(k)g^{-1}(k)(y_d(k+1) - f(k) - F(z)(\xi(k+1) + d(k+1))))$$
$$= -(1 - F(z))(\xi(k+1) + d(k+1)). \tag{18}$$

Define the Lyapunov function candidate $V(k) = e^2(k)$, and

$$V(k+1) - V(k)$$
$$= e^2(k+1) - e^2(k)$$
$$= \left((1 - F(z))(\xi(k+1) + d(k+1))\right)^2 - e^2(k)$$
$$\leq (1 - F(z))^2(|\xi(k+1)| + |d(k+1)|)^2 - e^2(k)$$
$$\leq (1 - F(z))^2(\xi_0 + d_0)^2 - e^2(k)$$
$$= (1 - F(z))^2\bar{\xi}^2 - e^2(k). \tag{19}$$

When $|e(k)| > |1 - F(z)|\bar{\xi}$, $V(k+1) - V(k) < 0$; therefore, the tracking error $e(k)$ is bounded by $\lim_{k\to\infty}|e(k)| \leq |1 - F(z)|\bar{\xi}$.

In fact, because the main focus of the paper is the application of the piezoelectric actuator in nanometer-scale ultraprecise tracking, the noise and disturbance is greatly diminished by fixing the experiment equipment on a vibration isolation mounting in a laboratory under precise environmental control. Besides, the modeling error can be progressively minimized via the updating of adaptive FHM. Hence, suitable filter can be chosen for both stability and excellent performance of the designed controllers in the practical tracking experiments.

IV. Experimental Results

As shown in Fig. 3, a nanopositioning stage driven by piezoelectric actuators (PICMA P-885.30) is built as the experimental platform. The piezoelectric actuator has a nominal displacement

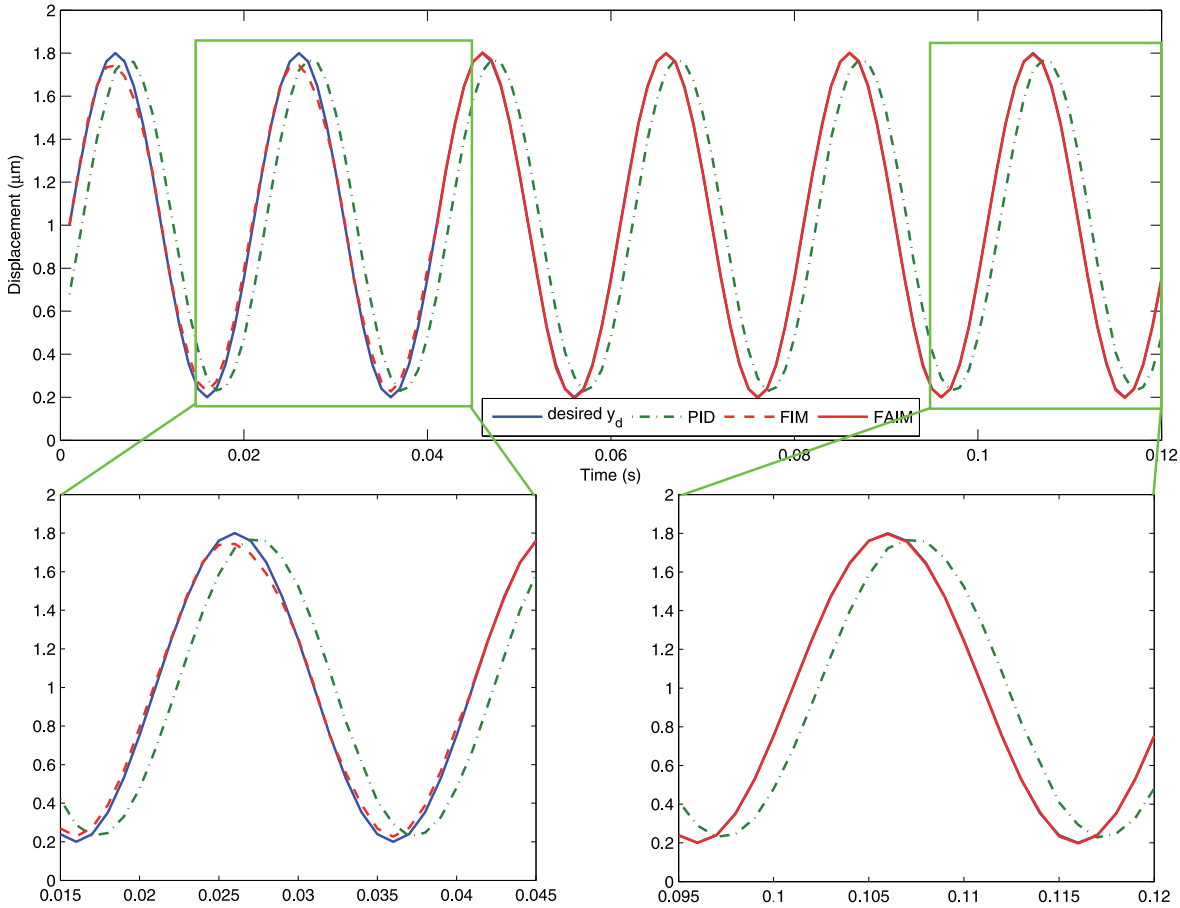

Fig. 7. Tracking results for 50-Hz sinusoidal waveform trajectory.

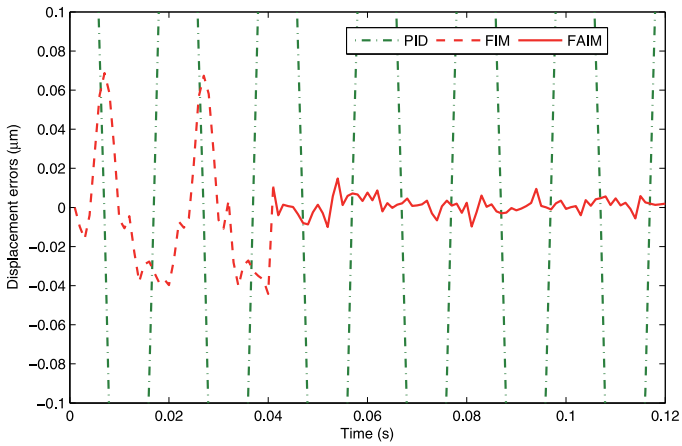

Fig. 8. Tracking errors for 50-Hz sinusoidal waveform trajectory.

of 0–10 μm and an operating voltage range from -20 to 120 V. Other experimental equipment includes a digital controller and built-in capacitive sensors (D-015.00). The digital controller consists of a floating-point DSP, a voltage amplifier (E-503.00) with 10$\times$ gain, a signal conditioner (E-509.C3A) for capacitive sensors, 16 bits A/D and 20 bits D/A converters. The floating-point DSP especially conducts the tracking control. The capacitive sensors have a displacement resolution less than 0.5 nm. The equipment mentioned above is mainly provided by Physik Instrumente GmbH & Co. KG in Germany. The experiment is carried out in a laboratory under precise environmental control, and the ambient temperature of the laboratory is kept at 22$\pm$0.5 °C. All the equipment is fixed on a vibration isolation mounting. The experimental sampling frequency is selected as 1 kHz, which means the sampling period T_s is 1 ms. The diagram of the experimental layout is illustrated in Fig. 4.

In tracking control applications of piezoelectric actuators, periodic waveforms are commonly used as desired trajectories. Two cases of waveforms are chosen as y_d: single-frequency sinusoidal and multiple-frequency sinusoidal waveforms. Single-frequency sinusoidal waveforms are widely used as a result of continuous differentiability. Multiple-frequency sinusoidal waveforms can exhibit rate-dependent hysteresis characteristics. These cases can comprehensively check the effectiveness of the designed controllers.

Three different controllers are used in our experiments: 1) PID controller; 2) FIM controller; and 3) FAIM controller. For each case, comparison experiments are conducted.

Controller parameters are $k_p = 0.2, k_i = 1.0, k_d = 0.1, L = 6, \beta = 0.9$, and $T_s = 1$ ms, respectively. The detail results are given as follows.

1) The parameters k_p, k_i, and k_d of the PID controller are chosen for both stability and performance of the system. Besides, the bandwidth of the system with the PID controller is guaranteed to be about 80 Hz for trajectory tracking.
2) As the key parameter of the FIM and FAIM controllers, L is chosen as a tradeoff between tracking performances

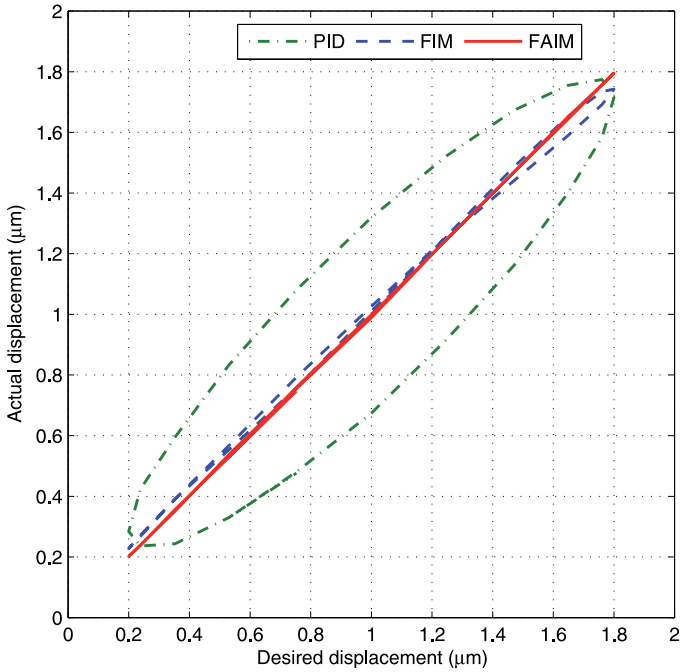

Fig. 9. Results of hysteresis effect compensations for 50-Hz sinusoidal waveform trajectory.

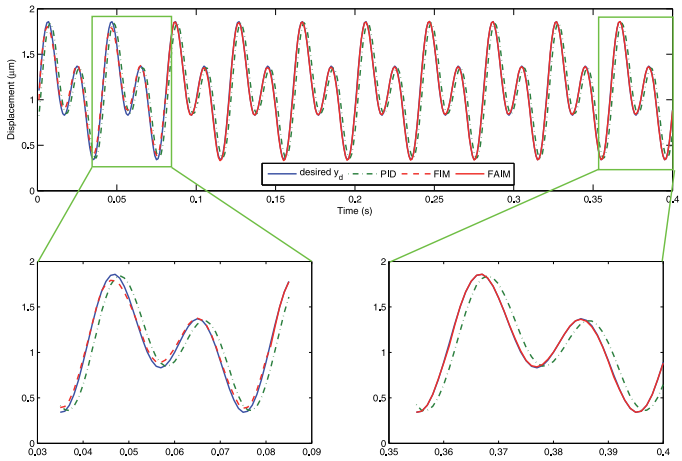

Fig. 10. Tracking results for multiple-frequency sinusoidal waveform trajectory.

and practical ease of real-time implementation. With such choice of $L = 6$, during each sampling period ($T_s = 1$ ms), $T_{\mathrm{FAIM}} \approx 7300$ and $T_{\mathrm{FIM}} \approx 80$. In practical experiments, the controllers are implemented via a 375-MHz TMS320C6748 floating-point DSP with up to 2746 million floating-point operations per second (MFLOPS). The DSP can at least perform 80 000 multiplication and division operations in 1 ms. Therefore, the designed controllers are practically feasible.

3) The parameter β of the feedback filter is chosen as $\beta = 0.9$ mainly for the closed-loop stability of the FIM and FAIM controllers.

At first, an experiment for showing the approximation performance of the proposed FHM is executed. Composed of different frequencies, the input voltage is chosen as $u_v(kT_s) = 1.5\exp(-2.5kT_s)(\sin(120\pi kT_s\exp(-1.2kT_s)) + 1) + 4$. Fig. 5 shows the result of comparing the measured hysteresis

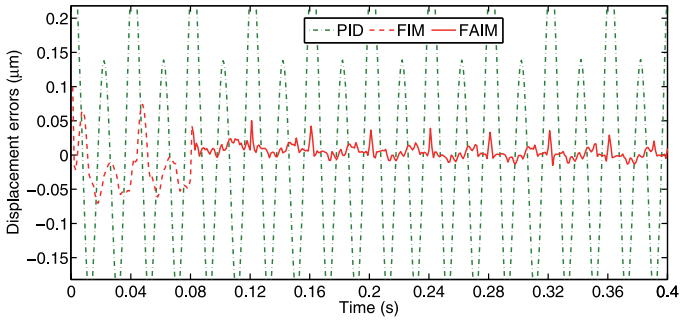

Fig. 11. Tracking errors for multiple-frequency sinusoidal waveform trajectory.

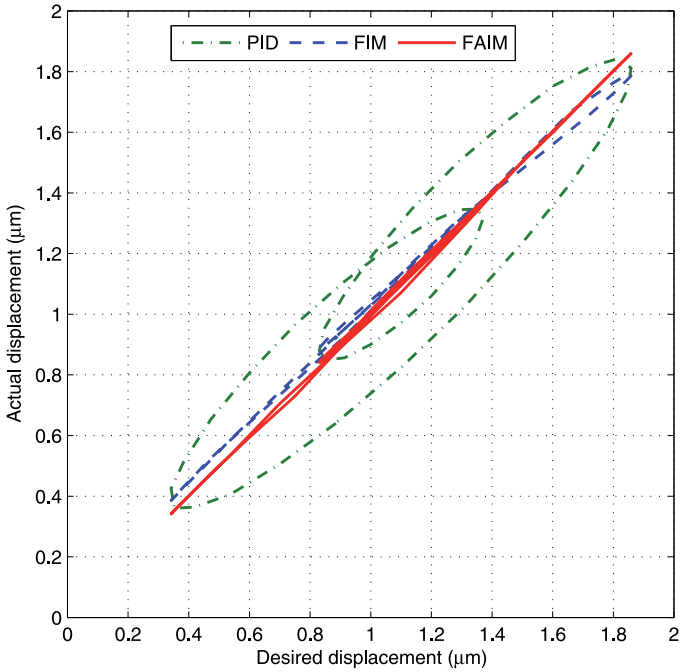

Fig. 12. Results of hysteresis effect compensations for multiple-frequency sinusoidal waveform trajectory.

curve with the approximated hysteresis curve from FHM. The maximum modeling error is 0.46%. Clearly, the result indicates that the developed FHM can effectively match the hysteresis of piezoelectric actuators.

The input voltage for initial FHM identification is shown in Fig. 6. It should be noted that the voltage is not amplified by the voltage amplifier.

A. *Single-Frequency Sinusoidal Waveform*

The desired trajectory is chosen as $y_d = 1.0 + 0.8\sin(100\pi t)$ μm, whose frequency is 50 Hz. In Figs. 7 and 8, tracking results and errors are compared among the PID, FIM, and FAIM controllers. As seen, the PID controller cannot compensate for the hysteresis effect at the high frequency of 50 Hz, while the FIM controller can achieve about five times better tracking performance than the PID controller. The maximum tracking error of the FIM controller is 68.7 nm, which needs to be further reduced by the FAIM controller. Being 92% less than 68.7 nm, the maximum tracking error of the FAIM controller at the last period of y_d is 5.8 nm. Fig. 9 shows the results of

TABLE I
TRACKING PERFORMANCES OF THREE DIFFERENT CONTROLLERS FOR TWO CASES OF TRAJECTORIES

Desired trajectory (μm)	Controller	e_{ma} [a] (nm)	e_{mr} [b] (%)	e_{rms} [c] (nm)
$y_d = 1.0 + 0.8\sin(100\pi t)$	PID	336.0	18.67	231.1
	FIM	68.7	3.82	33.8
	FAIM	5.8	0.32[d]	3.3
$y_d = 1.1 + 0.5\sin(100\pi t)$ $+0.35\sin(50\pi t)$	PID	290.6	15.64	155.9
	FIM	100.0	5.38	42.4
	FAIM	29.0	1.56	8.5

[a] $e_{\mathrm{ma}} = \max(|y_d - y|)$. [b] $e_{\mathrm{mr}} = \max(|y_d - y|) / \max(y_d)$. [c] $e_{\mathrm{rms}} = \sqrt{(\sum (y_d - y)^2)/N}$. [d] e_{mr} of other proposed controllers: 1.40% at 50 Hz [21]; 3.35% at 4 Hz [40]; 2.50% at 0.01 Hz [9].

hysteresis effect compensations of the controllers. The maximum tracking error obtained by the FAIM controller is 0.32%, while that achieved by [21] was 1.40% for 50 Hz (the same frequency) sinusoidal waveform trajectory. Besides, the maximum tracking error was 3.35% achieved by the model predictive output integral discrete-time sliding mode controller [40] for the 4-Hz trajectory; for lower frequency of 0.01 Hz, the maximum tracking error was 2.50% when the combined cascaded PD/lead-lag feedback controller with the feedforward hysteresis compensator [9] was applied. Clearly, the proposed FAIM controller can achieve nanometer-scale precision for high-speed tracking applications.

B. Multiple-Frequency Sinusoidal Waveform

Including 25- and 50-Hz frequency, the desired trajectory is $y_d = 1.1 + 0.5\sin(100\pi t) + 0.35\sin(50\pi t)$ μm. Figs. 10 and 11 show the tracking results and errors of the controllers, respectively. From Fig. 11, the maximum tracking error of the FIM controller is 100 nm, while that of the FAIM controller is 29 nm. Illustrated in Fig. 12, the multiloop rate-dependent hysteresis effect is greatly decreased by the FAIM controller. In fact, higher performance can be attained by choosing larger L at a slightly higher cost of real-time computational burden. Besides, more periods of y_d run better performance of the FAIM controller achieved.

In summary, tracking performances of the proposed three different controllers (PID, FIM, and FAIM) for the two cases of trajectories (50 and 50 + 25 Hz) are shown in Table I.

V. CONCLUSION

In this paper, an online T–S FHM is proposed for hysteresis in piezoelectric actuators. Based on the inverse of the developed FHM, an FIM controller is designed to decrease the hysteresis effect. To achieve nanometer-scale tracking precision, the FAIM controller is uniquely developed. Finally, the experimental results for two cases are shown: the first is with 50 Hz and the other with multiple-frequency sinusoidal trajectories tracking that demonstrate the nanometer-scale tracking performance of the novel FAIM controller. Especially, being 0.32% of the maximum desired displacement, the maximum error of 50-Hz sinusoidal tracking is greatly reduced to 6 nm. Nevertheless, further developments of the proposed control strategy will include: 1) more precise identification of FHM; 2) less computational time of FAIM controller; and 3) more systematic design and choice of feedback filter for both stability and performance of the FAIM controller.

ACKNOWLEDGMENT

The authors would like to appreciate the valuable and constructive comments from the anonymous reviewers.

REFERENCES

[1] H. C. Liaw and B. Shirinzadeh, "Robust adaptive constrained motion tracking control of piezo-actuated flexure-based mechanisms for micro/nano manipulation," *IEEE Trans. Ind. Electron.*, vol. 58, no. 4, pp. 1406–1415, Apr. 2011.

[2] C.-M. Lin and H.-Y. Li, "Intelligent control using the wavelet fuzzy CMAC backstepping control system for two-axis linear piezoelectric ceramic motor drive systems," *IEEE Trans. Fuzzy Syst.*, vol. 22, no. 4, pp. 791–802, Aug. 2014.

[3] Y. K. Yong, S. O. R. Moheimani, B. J. Kenton, and K. K. Leang, "High-speed flexure-guided nanopositioning: Mechanical design and control issues," *Rev. Sci. Instrum.*, vol. 83, pp. 121101-1–121101-22, 2012.

[4] L.-J. Lai, G.-Y. Gu, and L.-M. Zhu, "Design and control of a decoupled two degree of freedom translational parallel micro-positioning stage," *Rev. Sci. Instrum.*, vol. 83, pp. 045 105–045 105–17, 2012.

[5] X. L. Dean-Ben and D. Razansky, "Adding fifth dimension to optoacoustic imaging: Volumetric time-resolved spectrally enriched tomography," *Light: Sci. Appl.*, vol. 3, p. e137, 2014.

[6] N. Accanto, J. B. Nieder, L. Piatkowski, M. Castro-Lopez, F. Pastorelli, D. Brinks, and N. F. van Hulst, "Phase control of femtosecond pulses on the nanoscale using second harmonic nanoparticles," *Light: Sci. Appl.*, vol. 3, p. e143, 2014.

[7] P. Ge and M. Jouaneh, "Tracking control of a piezoceramic actuator," *IEEE Trans. Control Syst. Technol.*, vol. 4, no. 3, pp. 209–216, May 1996.

[8] I. D. Mayergoyz, "Dynamic Preisach models of hysteresis," *IEEE Trans. Magn.*, vol. 24, no. 6, pp. 2925–2927, Nov. 1988.

[9] G. Song, J. Zhao, X. Zhou, and J. A. D. Abreu-Garcia, "Tracking control of a piezoceramic actuator with hysteresis compensation using inverse Preisach model," *IEEE/ASME Trans. Mechatron.*, vol. 10, no. 2, pp. 198–209, Apr. 2005.

[10] S. Bobbio, G. Miano, C. Serpico, and C. Visone, "Models of magnetic hysteresis based on play and stop hysterons," *IEEE Trans. Magn.*, vol. 33, no. 6, pp. 4417–4426, Nov. 1997.

[11] M. Goldfarb and N. Celanovic, "Modeling piezoelectric stack actuators for control of micromanipulation," *IEEE Control Syst. Mag.*, vol. 17, no. 3, pp. 69–79, Jun. 1997.

[12] L. O. Chua and S. C. Bass, "A generalized hysteresis model," *IEEE Trans. Circuit Theory*, vol. CT-19, no. 1, pp. 36–48, Jan. 1972.

[13] J. Oh and D. S. Bernstein, "Semilinear Duhem model for rate-independent and rate-dependent hysteresis," *IEEE Trans. Automat. Control*, vol. 50 , no. 5, pp. 631–645, May 2005.

[14] D. Jiles and J. Thoelke, "Theory of ferromagnetic hysteresis determination of model parameters from experimental hysteresis loops," *IEEE Trans. Magn.*, vol. 25, no. 5, pp. 3928–3930, Sep. 1989.

[15] L. Deng and Y. Tan, "Diagonal recurrent neural network with modified backlash operators for modeling of rate-dependent hysteresis in piezoelectric actuators," *Sensors Actuators A, Phys.*, vol. 148, no. 1, pp. 259–270, 2008.

[16] W. T. Ang, P. K. Khosla, and C. N. Riviere, "Feedforward controller with inverse rate-dependent model for piezoelectric actuators in trajectory-tracking applications," *IEEE/ASME Trans. Mechatron.*, vol. 12, no. 2, pp. 134–142, Apr. 2007.

[17] M. A. Janaideh, S. Rakheja, and C.-Y. Su, "An analytical generalized Prandtl–Ishlinskii model inversion for hysteresis compensation in micropositioning control," *IEEE/ASME Trans. Mechatron.*, vol. 16, no. 4, pp. 734–744, Aug. 2011.

[18] Y. Cao and X. B. Chen, "A novel discrete ARMA-based model for piezoelectric actuator hysteresis," *IEEE/ASME Trans. Mechatron.*, vol. 17, no. 4, pp. 737–744, Aug. 2012.

[19] Y. L. Zhang, M. L. Han, M. Y. Yu, C. Y. Shee, and W. T. Ang, "Automatic hysteresis modeling of piezoelectric micromanipulator in vision-guided micromanipulation systems," *IEEE/ASME Trans. Mechatron.*, vol. 17, no. 3, pp. 547–553, Jun. 2012.

[20] S. Tien, Q. Zou, and S. Devasia, "Iterative control of dynamics-coupling-caused errors in piezoscanners during high-speed AFM operation," *IEEE Trans. Control Syst. Technol.*, vol. 13, no. 6, pp. 921–931, Nov. 2005.

[21] S. Bashash and N. Jalili, "Robust multiple frequency trajectory tracking control of piezoelectrically driven micro/nanopositioning systems," *IEEE Trans. Control Syst. Technol.*, vol. 15, no. 5, pp. 867–878, Sep. 2007.

[22] C.-L. Hwang and C. Jan, "Optimal and reinforced robustness designs of fuzzy variable structure tracking control for a piezoelectric actuator system," *IEEE Trans. Fuzzy Syst.*, vol. 11, no. 4, pp. 507–517, Aug. 2003.

[23] G. Song, V. Chaudhry, and C. Batur, "Precision tracking control of shape memory alloy actuators using neural networks and a sliding-mode based robust controller," *Smart Mater. Struct.*, vol. 12, pp. 223–231, 2003.

[24] P.-B. Nguyen and S.-B. Choi, "Compensator design for hysteresis of a stacked PZT actuator using a congruency-based hysteresis model," *Smart Mater. Struct.*, vol. 21, pp. 015009-1–015009-9, 2012.

[25] P.-K. Wong, Q. Xu, C.-M. Vong, and H.-C. Wong, "Rate-dependent hysteresis modeling and control of a piezostage using online support vector machine and relevance vector machine," *IEEE Trans. Ind. Electron.*, vol. 59, no. 4, pp. 1988–2001, Apr. 2012.

[26] W. F. Xie and A. B. Rad, "Fuzzy adaptive internal model control," *IEEE Trans. Ind. Electron.*, vol. 47, no. 1, pp. 193–202, Feb. 2000.

[27] R. Boukezzoula, S. Galichet, and L. Foulloy, "Nonlinear internal model control: application of inverse model based fuzzy control," *IEEE Trans. Fuzzy Syst.*, vol. 11, no. 6, pp. 814–829, Dec. 2003.

[28] G. Tsekouras, H. Sarimveis, and G. Bafas, "A simple algorithm for training fuzzy systems using input-output data," *Advances Eng. Softw.*, vol. 34, pp. 247–259, 2003.

[29] A. Adly and S. Abd-El-Hafiz, "Efficient modeling of vector hysteresis using fuzzy inference systems," *Phys. B*, vol. 403, pp. 3812–3818, 2008.

[30] P. Li, F. Yan, C. Ge, X. Wang, L. Xu, J. Guo, and P. Li, "A simple fuzzy system for modelling of both rate-independent and rate-dependent hysteresis in piezoelectric actuators," *Mech. Syst. Signal Process.*, vol. 36, no. 1, pp. 182–192, Mar. 2013.

[31] G. Feng, "A survey on analysis and design of model-based fuzzy control systems," *IEEE Trans. Fuzzy Syst.*, vol. 14, no. 5, pp. 676–697, Oct. 2006.

[32] L.-X. Wang, "Stable adaptive fuzzy control of nonlinear systems," *IEEE Trans. Fuzzy Syst.*, vol. 1, no. 2, pp. 146–155, May 1993.

[33] S. Yordanova, D. Merazchiev, and L. Jain, "A two-variable fuzzy control design with application to an air-conditioning system," *IEEE Trans. Fuzzy Syst.*, vol. 23, no. 2, pp. 474–481, Apr. 2015.

[34] R. Qi, G. Tao, B. Jiang, and C. Tan, "Adaptive control schemes for discrete-time T-S fuzzy systems with unknown parameters and actuator failures," *IEEE Trans. Fuzzy Syst.*, vol. 20, no. 3, pp. 471–486, Jun. 2012.

[35] J. Dong and G.-H. Yang, "Reliable state feedback control of T-S fuzzy systems with sensor faults," *IEEE Trans. Fuzzy Syst.*, vol. 23, no. 2, pp. 421–433, Apr. 2015.

[36] T. Takagi and M. Sugeno, "Fuzzy identification of systems and its applications to modeling and control," *IEEE Trans. Syst., Man Cybern.*, vol. SMC-15, no. 1, pp. 116–132, Jan. 1985.

[37] Q. Gao, L. Liu, G. Feng, Y. Wang, and J. Qiu, "Universal fuzzy integral sliding-mode controllers based on T-S fuzzy models," *IEEE Trans. Fuzzy Syst.*, vol. 22, no. 2, pp. 350–362, Apr. 2014.

[38] S. G. Devi, K. Selvam, and D. S. P. Rajagopalan, "An abstract to calculate big O factors of time and space complexity of machine code," in *Proc. 2nd Int. Conf. Sustainable Energy Intell. Syst.*, Jul. 2011, pp. 844–847.

[39] K. H. Ang, G. Chong, and Y. Li, "PID control system analysis, design, and technology," *IEEE Trans. Control Syst. Technol.*, vol. 13, no. 4, pp. 559–576, Jul. 2005.

[40] Q. Xu and Y. Li, "Micro-/Nanopositioning using model predictive output integral discrete sliding mode control," *IEEE Trans. Ind. Electron.*, vol. 59, no. 2, pp. 1161–1170, Feb. 2012.